Available online at www.sciencedirect.com

ScienceDirect

Procedia Engineering 10 (2011) 3775–3786

Engineering Procedia

ICM11

Influence of the Resin Layer Thickness at the Interface of Hybrid Metal-composite Co-cured Joints

Andrea Russo[a], Bernardo Zuccarello[b]*

[a]*Alenia Aermacchi, Via Ing. P. Foresio 1, 21040 Venegono Superiore (VA), Italy*
[b]*Università di Palermo - Dipartimento di Ingegneria, Viale delle Scienze, 90128 Palermo, Italy*

Abstract

As discussed in literature, the accurate analysis of the modern co-cured joints between composite materials or between a metal and a composite material (hybrid joints) is complicated by the influence of the interface resin layer on the interface singular stress field. In such joints, in fact, there is not a proper adhesive layer and the thickness of the resin layer, that plays the role of the adhesive, is not constant due to the presence of the reinforcing fibers in the composite adherent. For this reason several authors assume that a generic co-cured joint can not be studied as a simple bi-material joint, without considering the particular characteristics of the actual resin layer. This problem is also involved into the development of reliable design methods able to give accurate predictions of the joint efficiency. In this work, by theoretical analyses performed by using the Lekhnitskii theory, numerical simulations carried out by means of the boundary element method and experimental investigations based on the combined use of the generalized Dundurs parameters and digital photoelasticity, the influence of the resin layer on the singular stress field at the interface of a generic hybrid metal-composite joint, has been investigated.

Keywords: co-cured joint; composite material; photoelasticity; stress intensity factor.

1. Introduction

A co-cured joint is a bonded joint between two composite adherents or a composite adherent and a metal adherent in which the adhesive role is played by the resin of the composite adherent; unlike a classical adhesively bonded joint, in the co-cured joint it is not easy to distinguish the adhesive layer between the adherents. As a consequence, the resin thickness at the interface cannot be assumed as a joint design parameter, since the thickness cannot be controlled during the manufacturing of the joint, depending by several factors as manufacturing process, cure conditions, etc. Although in co-cured joints the thickness of the interface resin layer is usually very low if

* Corresponding author: Bernardo Zuccarello. Tel.: +39-91-6657102; fax: +9-91-484334.
E-mail address: zuccarello@dima.unipa.it.

1877-7058 © 2011 Published by Elsevier Ltd. Selection and peer-review under responsibility of ICM11
doi:10.1016/j.proeng.2011.04.617

compared to the typical thicknesses of the adhesive layers of classical adhesively bonded joints, this thickness is not negligible in many cases as low pressure curing, adhesive film interposed between the adherents or adhesive film with embedded reinforcing grid. In this last particular case, the thickness of the interface resin layer can be easily assumed as design variable being it almost equal to the reinforcing grid thickness [1]. Also, in single and double lap joints the cohesive failures of the thin interface resin layer as well as of the first lamina of the composite adherent, have shown that the metal-composite interface is often an interface of resin mixed with fibers [2-6].
In order to evaluate the accuracy of a theoretical design method that consider the joint as a simple biomaterial system and relates the failure load to the stress intensity factors that govern the singular stress field at the interface, in this paper the influence of the resin layer thickness between the adherents as been investigated by using theoretical analyses, numerical simulations and experimental assessments.

1.1. State of the art

The influence of the adhesive layer on the singular stress field that occurs in bi-material joints has been investigated in literature by many authors. In detail, in [7,8] the authors have studied the singular stress field that occurs at the tip of an interface crack in a bi-material joint; in [9] the authors have demonstrated that in the experimental practice it is possible to neglect the influence of the interface adhesive layer by using an adhesive with the same elastic properties of one of the materials joined. Other authors have studied the adhesive bonded joints following the approach of fracture mechanics [10,11]. Among them, some authors have investigated the influence of the adhesive layer thickness on the stress intensity factors at the crack tip. Trantina G.G. [10] has investigated the use of the fracture mechanics approach to study an aluminum-epoxy resin-aluminum joint notched along the interface and loaded in opening mode (mode I). Using finite element analyses, Trantina has investigated the variation of strain energy rate G and then the influence on the stress intensity factor K versus the thickness of the adhesive layer. Trantina concluded that for very small adhesive thicknesses, the value of the strain energy of the bi-material system analyzed is approximated by the strain energy for the homogeneous system (aluminum only), $G_{Al\text{-}Ep} \approx G_{Al}$, while the ratio of the stress intensity factors for homogeneous and bi-material systems is approximately equal to the square root of the Young moduli ratio of adherent and adhesive, i.e. $K_{Al}/K_{Al,Ep} \approx (E_{Al}/E_{Ep})^{1/2}$.
In case of an interface semi-infinite crack, Suo and Hutchinson [11,12] present a series of theoretical papers in which the stress intensity factors are determined in closed form for a sandwich type bi-material joint, in which the adhesive is inserted between two sheets of homogeneous material. The proposed expressions are valid for notched specimens, for which K_I and K_{II} are known in the homogeneous case, as well as for asymptotic problems, that is for joints where the thickness h of the adhesive is much lower than the dimensions of the joint. While Suo and Hutchinson [11] considered the crack at the interface between adhesive and adherent, Santhanam [13], by means of numerical analyses, considers the same configurations but with crack contained in the adhesive layer. Therefore, in [13] Santhanam, by considering a tri-material joint (material 1- adhesive - material 2), compares his results with those given by Rice [14] for a simple bi-material joint (material 1- material 2) in the case of central crack at the interface, reporting differences lesser than 2% for the real part of the SIF K_1; higher differences are observed in determining the imaginary part of the SIF K_2 mainly due to the fact that K_2 is, for the cases analyzed, two orders of magnitude lower than K_1. In the case of semi-infinite interface crack in a bending specimen, the differences for both real part and imaginary part of the complex expression of the stress intensity factor are small if compared to the numerical results provided by Charalambides et al. [15], who studied the simple bi-material case (without adhesive).
Moreover, Crews et al. [16] studied numerically the influence that some characteristic parameters may have on the singular stress field at the crack tip in the double cantilever beam (DCB) joints. In detail, they analyzed the case of adherents made of carbon fiber-epoxy resin and epoxy adhesive, varying the adhesive thickness t. In detail, they consider the adhesive thickness that varies from 0.01 mm (common case of co-cured joints) to 0.66 mm (starting from t = 0.1 mm it is possible to speak of bonded joints). They observe that the curve of the peeling stress near the crack tip does not depend on the adhesive thickness, while different curves are obtained away from the crack tip. This means that the specimens studied have the same stress intensity factors varying the adhesive thickness.
In [17] Penada modifies the homogeneous solution obtained by Kanninen [18] and obtains a closed-form expression for G by considering a DCB specimen with adhesive layer. He analyzes the case of orthotropic composite specimens and compares the results with the exact solution obtained by Suo et al. [19] for the case of specimen without adhesive. The results show that the proposed method agrees well with numerical simulations and, by reducing the

thickness of the adhesive layer, the stress intensity factors tends to the theoretical solution obtained for the bi-material specimen (see Suo [19]).
In [20,21] Wang and Agrawal published a series of works in which they modify the solution obtained by Suo and Hutchinson [11] for the closed form determination of *K* for a bi-layer compact sandwich (BCS). In addition, they carry out numerical analyses to investigate the effects of the adhesive thickness on *K* and propose a correction factor to correct the proposed solution. The results show that the proposed corrected solution tends to the solution for homogeneous material when the adhesive thickness decreases, or the mismatch of the elastic properties of adherents and adhesive decrease.

2. Theoretical analysis

The approach of the complex potentials for anisotropic bodies was introduced by Lekhnitskii [22], Eshelby et al. [23] and Stroh [24]. For convenience, the work of these authors are often referred to by the acronym LES. For a homogeneous material for which the *xy* plane is an isotropy plane, the characteristic equation for plane strain state is [22]:

$$l_4(\mu) \equiv s_{11}\mu^4 - 2s_{16}\mu^3 + (2s_{12} + s_{66})\mu^2 - 2s_{26}\mu + s_{22} = 0 \tag{1}$$

where s_{ij} are the strain coefficients. It has been shown by Lekhnitskii [22] that the roots of equation *(1)* can never be real: these roots are two pairs of complex and conjugate solutions. Assuming that they are distinct, it is possible to choose two distinct roots, μ_1 and μ_2, with positive imaginary part, each associated with a complex variable $z_j = x + \mu_j y$. The stress/displacement field can be expressed by two holomorphic functions $\phi_1(z_1)$ and $\phi_2(z_2)$, whereas the complex numbers μ_1 and μ_2 depend on the material characteristics. The way to obtain these numbers was proposed by Eshelby et al. [23] and Lekhnitskii [22], then it was summarized by Suo [7]. For orthotropic materials, μ_j are the roots with positive imaginary part of the equation of fourth order [7]:

$$\lambda\,\mu^4 + 2\rho\,\lambda^{\frac{1}{2}}\mu^2 + 1 = 0 \tag{2}$$

which is valid for both plane stress and plane strain state. For plane stress, the constants λ and ρ that provide a measure of the material anisotropy is given by:

$$\lambda = \frac{s_{11}}{s_{22}}, \qquad \rho = \frac{1}{2}(2s_{12} + s_{66})(s_{11}s_{22})^{-1/2} \tag{3}$$

The plane strain state is obtained by substituting for s_{ij} the reduced coefficients:

$$s'_{ij} = s_{ij} - \frac{s_{i3}s_{j3}}{s_{33}} \tag{4}$$

The general expressions of the complex numbers are:

$$\begin{aligned} &\mu_1 = i\lambda^{-\frac{1}{4}}(n+m),\ \ \mu_2 = i\lambda^{-\frac{1}{4}}(n-m) && \text{for } 1 < \rho < \infty \\ &\mu_1 = \lambda^{-\frac{1}{4}}(in+m),\ \ \mu_2 = \lambda^{-\frac{1}{4}}(in-m) && \text{for } -1 < \rho < 1 \\ &\mu_1 = \mu_2 = i\lambda^{-\frac{1}{4}} && \text{for } \rho = 1 \end{aligned} \tag{5}$$

where

$$n = \left[\frac{1}{2}(1+\rho)\right]^{\frac{1}{2}}, \qquad m = \left[\frac{1}{2}(1-\rho)\right]^{\frac{1}{2}} \tag{6}$$

Since the strain energy is positive, it follows that $\lambda>0$ and $-1<\rho<\infty$. In detail, for a generic isotropic materials $\lambda = \rho = 1$ and $\mu_1 = \mu_2 = i$. The displacements u_i, the stresses σ_{ij} and the resultant forces T_i can be obtained through the complex potentials as:

$$u_i = 2\,\mathrm{Re}\left\{\sum_{j=1}^{2} A_{ij}\Phi_j(z_j)\right\}, \qquad T_i = -2\,\mathrm{Re}\left\{\sum_{j=1}^{2} L_{ij}\Phi_j(z_j)\right\} \tag{7}$$

$$\sigma_{2i} = 2\,\mathrm{Re}\left\{\sum_{j=1}^{2} L_{ij}\Phi'_j(z_j)\right\}, \qquad \sigma_{1i} = -2\,\mathrm{Re}\left\{\sum_{j=1}^{2} L_{ij}\mu_j\Phi'_j(z_j)\right\} \tag{8}$$

where Φ' is the derivative of Φ. For anisotropic materials, the general expressions of the matrices [A] and [L] are provided by Lekhnitskii [22]. For orthotropic materials, they can be simplified as:

$$[A]=\begin{pmatrix} s_{11}\mu_1^2+s_{12} & s_{11}\mu_2^2+s_{12} \\ s_{21}\mu_1+\dfrac{s_{22}}{\mu_1} & s_{21}\mu_2+\dfrac{s_{22}}{\mu_2} \end{pmatrix} \qquad [L]=\begin{pmatrix} -\mu_1 & -\mu_2 \\ 1 & 1 \end{pmatrix} \tag{9}$$

In order to define the stress/displacement field for isotropic materials, Stroh [24] introduced the relation between LES and isotropic complex potentials of Muskhelishvili [25] through the positive Hermitian matrix:

$$[B]=\begin{pmatrix} 2n\lambda^{\frac{1}{4}}\left(s_{11}s_{22}\right)^{\frac{1}{2}} & i\left(\left(s_{11}s_{22}\right)^{\frac{1}{2}}+s_{12}\right) \\ -i\left(\left(s_{11}s_{22}\right)^{\frac{1}{2}}+s_{12}\right) & 2n\lambda^{-\frac{1}{4}}\left(s_{11}s_{22}\right)^{\frac{1}{2}} \end{pmatrix} \tag{10}$$

It is interesting to note that [B] is valid for isotropic materials also, for which $\rho=1$ ([A] and [L] are singular).
For joints made by two orthotropic materials, M_1 and M_2, it is possible to define two bi-material matrix [H] and [G], which are positive Hermitian matrices, containing the elastic constants of both materials:

$$[H]=[B]_{M_1}+[B]_{M_2} \qquad [G]=[B]_{M_1}-[B]_{M_2} \tag{11}$$

The matrix [H] for two orthotropic material with principal axes aligned is:

$$[H]=H_{11}\begin{pmatrix} 1 & -i\beta\left(\dfrac{H_{22}}{H_{11}}\right)^{\frac{1}{2}} \\ i\beta\left(\dfrac{H_{22}}{H_{11}}\right)^{\frac{1}{2}} & \dfrac{H_{22}}{H_{11}} \end{pmatrix} \tag{12}$$

where

$$\begin{cases} H_{11}=\left[2n\lambda^{\frac{1}{4}}\left(s_{11}s_{22}\right)^{\frac{1}{2}}\right]_{M_1}+\left[2n\lambda^{\frac{1}{4}}\left(s_{11}s_{22}\right)^{\frac{1}{2}}\right]_{M_2} \\ H_{22}=\left[2n\lambda^{-\frac{1}{4}}\left(s_{11}s_{22}\right)^{\frac{1}{2}}\right]_{M_1}+\left[2n\lambda^{-\frac{1}{4}}\left(s_{11}s_{22}\right)^{\frac{1}{2}}\right]_{M_2} \\ \left(H_{11}H_{22}\right)^{\frac{1}{2}}\beta=\left[\left(s_{11}s_{22}\right)^{\frac{1}{2}}+s_{12}\right]_{M_2}-\left[\left(s_{11}s_{22}\right)^{\frac{1}{2}}+s_{12}\right]_{M_1} \end{cases} \tag{13}$$

The constant β is the generalization of the Dundurs parameter [26]. Not-oscillatory fields can be obtained if [H] is real, or if $\beta=0$. Therefore, considering the case $\beta\neq0$, an oscillatory index ε is defined as:

$$\varepsilon=\frac{1}{2\pi}\ln\left(\frac{1-\beta}{1+\beta}\right) \tag{14}$$

For orthotropic materials, the second bi-material matrix [G] becomes:

$$[G]=H_{11}\begin{pmatrix} \alpha_1 & -i\beta\left(\dfrac{H_{22}}{H_{11}}\right)^{\frac{1}{2}} \\ i\beta\left(\dfrac{H_{22}}{H_{11}}\right)^{\frac{1}{2}} & \alpha_2 \end{pmatrix} \tag{15}$$

where two additional generalized Dundurs parameters are shown, α_1 and α_2.
Obviously, they are reduced to α_{iso} when both materials M_1 and M_2 are isotropic. A fourth parameter appears in the matrices [H] and [G], which is reduced to the unit for isotropic materials. For orthotropic materials α_1 and α_2 are defined as follows:

$$\alpha_1=\frac{\left[2n\lambda^{\frac{1}{4}}\left(s_{11}s_{22}\right)^{\frac{1}{2}}\right]_B-\left[2n\lambda^{\frac{1}{4}}\left(s_{11}s_{22}\right)^{\frac{1}{2}}\right]_A}{H_{11}} \tag{16}$$

$$\alpha_2=\frac{\left[2n\lambda^{-\frac{1}{4}}\left(s_{11}s_{22}\right)^{\frac{1}{2}}\right]_B-\left[2n\lambda^{-\frac{1}{4}}\left(s_{11}s_{22}\right)^{\frac{1}{2}}\right]_A}{H_{11}} \tag{17}$$

Generally, for orthotropic materials $\lambda^{1/4}$ is close to the unit and, therefore, α_1 and α_2 are almost equal. In this case it is possible to obtain an average value of α, which is the arithmetic average value of α_1 and α_2:

$$\alpha = \frac{\left[n\left(\lambda^{\frac{1}{4}} + \lambda^{-\frac{1}{4}}\right)\left(s_{11}s_{22}\right)^{\frac{1}{2}}\right]_B - \left[n\left(\lambda^{\frac{1}{4}} + \lambda^{-\frac{1}{4}}\right)\left(s_{11}s_{22}\right)^{\frac{1}{2}}\right]_A}{H_{11}} \tag{18}$$

As an alternative to α, another generalized Dundurs parameter Σ can be defined as:

$$\Sigma = \frac{\left[\left(s_{11}s_{22}\right)^{\frac{1}{2}}\right]_B}{\left[\left(s_{11}s_{22}\right)^{\frac{1}{2}}\right]_A} = \frac{(1+\alpha)}{(1-\alpha)} \tag{19}$$

Like α, the parameter Σ measures the relative stiffness of the two coupled materials.

Cherkaev et al. [27] have shown that for boundary conditions of simple tension, the stress field in an anisotropic elastic body with a variety of discontinuous interface conditions (including the simply connection) is invariant with an appropriate constant change (a scalar multiple of the fourth order rotation tensor) of the elastic compliance. It is noted that, under these conditions, the parameters λ and ρ, the complex roots μ_j, H_{11} and H_{22}, β, as well as the oscillatory index ε, are invariant (Gosz and Moran, [28]).

Suo [7] has also noted that, for a composite made by two aligned orthotropic materials with the boundary conditions of tension, α and β (or ε and Σ) together with the two anisotropy measures, λ and ρ (for each material), are all needed for the characterization of the stress field.

Such an approach can be useful in experimental analysis of anisotropic materials joints (*amj*). In fact, in order to investigate the stress field at the interface between two anisotropic materials near the free edges, by using the photoelasticity it is possible to study a photoelastic equivalent joint (*pej*) made by one or two isotropic birefringence materials (see fig.1), characterized by the same generalized Dundurs parameters:

$$(\alpha, \beta, \lambda, \rho)_{pej.} \equiv (\alpha, \beta, \lambda, \rho)_{amj} \tag{20}$$

The photoelastic analysis may also be useful to investigate the influence of the resin layer between the two materials joined, which is often neglected in numerical analyses of co-cured composite joints. In fact, a composite laminate made by n laminas is constituted by $2n+1$ layers of fiber and resin and it is generally analyzed by considering its global elastic properties obtained by the TCL, i.e. by neglecting the actual layer of resin between the two materials joined.

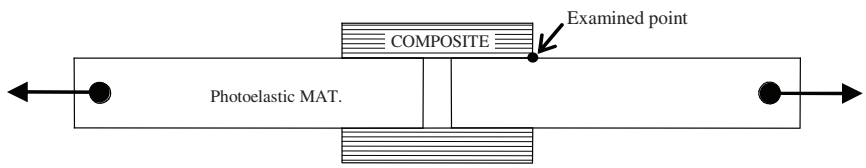

Fig. 1 – Double lap co-cured joint used for the photoelastic analysis.

3. Numerical analysis

In order to provide a contribution to the study of the influence of the interface resin layer on the Generalized Stress Intensity Factors (GSIFs) that govern the singular stress field at the interface of a generic co-cured joint, numerical investigations have been carried out on a double lap co-cured joint aluminum-CFRP (see fig. 2). The numerical model is a 2D plane model made by the boundary element code Beasy®, using quadratic elements, with a very graded mesh near the singularity points (intersection between interface and free edge) in order to obtain a minimum size of the elements equal to 1 μm. The numerical model also considers a layer of epoxy resin between the adherents.

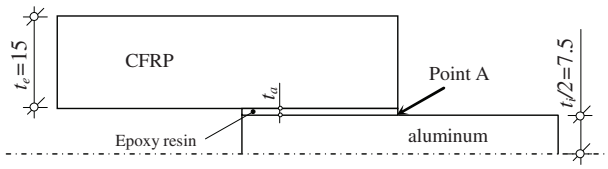

Material	E_L [GPa]	E_T, E_Z [GPa]	G_{LT} [GPa]	ν_{LT}
CFRP	121.56	6.16	2.235	0.29
Aluminum	72	-	-	0.29
Epoxy resin	3.1	-	-	0.38

Fig. 2 –Boundary element model of a double lap co-cured joint with interface resin layer; material properties table.

Analyses were performed by varying the thickness of the interface resin layer t_a. The relative results were compared with those obtained by a similar model of a simplified co-cured joint, i.e a joint without adhesive resin layer (t_a=0).

Fig. 3 shows the peeling stress σ_y near point A (see fig.2). This figure shows that in practice it is not possible to distinguish the curves relative to t_a = 0.01 mm from that relative to t_a = 0, i.e. relative to an ideal co-cured joint without interface resin layer. On the contrary, the curve relative to a joint with t_a = 0.6 mm is appreciably different, indicating that from this t_a value the influence of the interface resin layer becomes significant.

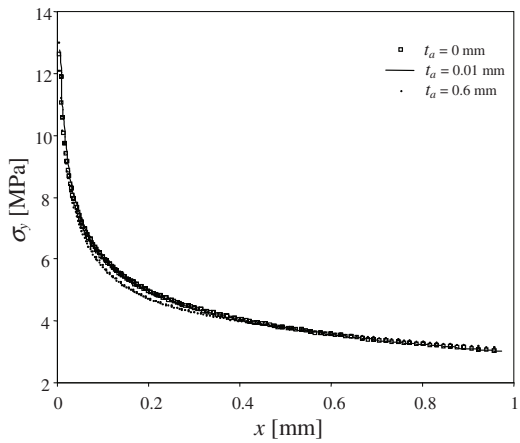

Fig. 3 – Peeling stress σ_y near point A for a double lap co-cured aluminum-unidirectional CFRP joint.

Moreover, as it is well known, the singular stress field near the point A (see fig.2) is in general described by a binomial equation when the singular stress field is described by two singularity orders in the section plane [25,29]:

$$\sigma_{ij}(r,\vartheta) = K_1 \cdot r^{-\omega_1} \cdot f_{ij,1}(\vartheta) + K_2 \cdot r^{-\omega_2} \cdot f_{ij,2}(\vartheta) \qquad (21)$$

where K_i are the stress intensity factors, ω_i are the singularity order, $f_{ij}(\theta)$ are the angular functions (i,j=1,2).

The binomial Eq.(*21*) becomes monomial when the singular stress field is described by only one singularity order, i.e:

$$\sigma_{ij}(r,\vartheta) = K_1 \cdot r^{-\omega_1} \cdot f_{ij,1}(\vartheta) \qquad (22)$$

Therefore, as in MFLE, once singularity orders and angular functions are analytically evaluated, the corresponding generalized stress intensity factors in the plane (in-plane GSIFs) can be computed numerically from the stress field near the singular point examined. It is also noted that, similarly to MFLE, the stress intensity factors K_{ij} can be written as [30-32]:

$$K_{ij} = \beta_{ij}\, \sigma_o w^{-\omega_{ij}} \qquad (i=1, 2;\ j=A, B) \qquad (23)$$

where σ_o is the applied remote stress, β_{ij} is the shape function (or dimensionless GSIF) that takes into account the geometry and the loading condition, w is a characteristic dimension of the joint, in the follow assumed to be equal to the thickness of the metal adherent. The shape function β_{SF} that governs the singular stress field near point A (monomial case) are reported in fig. 4, varying the thickness of the interface resin layer.

It is important to observe that the β_{SF} values decrease with the thickness of the interface resin layer for t_a<0.1 mm,

while they increase for t_a>0.1 mm.

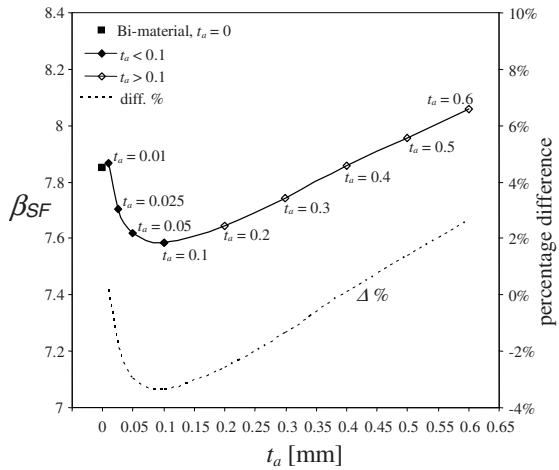

Fig. 4 – Shape function β_{SF} at the interface near the free edge of the CFRP, versus the thickness of the interface resin layer.

Consequently, it is possible to state that the value t_a = 0.1 mm can be considered as the frontier between classical adhesively bonded joints (t_a >0.1 mm) and the co-cured joints (t_a<0.1 mm) [16]. It is possible to note that, as confirmed also by the results of fig. 3, the shape functions values relative to joints with t_a =0 mm (ideal bi-material joint) and t_a =0.01 mm (actual co-cured joints) are almost coincident (Δ% <0.2%). In detail, fig. 4 shows that for any co-cured joint (t_a <0.1 mm) the percentage difference between the shape function values calculated for joint with an interface resin layer and those calculated for the ideal co-cured joint is in practice always less than ± 3%. In other words, the obtained results show that, in the analysis of co-cured joints the error due to neglecting the influence of the interface resin layer, is in general negligible.

4. Experimental analysis

In order to study the influence of the interface resin layer on the GSIFs of composite co-cured joints, as well as in order to set up a useful procedure for the experimental determination of the GSIFs of joints between anisotropic materials, by means of the combined use of the generalized Dundurs parameters and the photoelastic digital technique, some photoelastic analyses have been performed by varying the main influent factors.
In detail, through the digital photoelasticity, a double lap joint having the inner adherent of araldite and the outer adherent of GFRP unidirectional laminate, has been analyzed. Mechanical and photoelastic properties of the adherents are shown in Table 1.

Table 1. Properties of GFRP-araldite examined joint

Material	E_L [GPa]	E_T [GPa]	G_{LT} [GPa]	ν_{LT}	C [MPa^{-1}]
GFRP	28.5	3	2	0.3	-
araldite B CT200	3.5	-	-	0.4	58 · 10-6

It is to be noted that, regarding the singular stress field at the interface between the adherents (near the free edges), this joint is equivalent to the CFRP-GFRP co-cured joint having the mechanical properties shown in Table 2.

Table 2. Mechanical properties of the CFRP-GFRP joint

Material	E_L [GPa]	E_T [GPa]	G_{LT} [GPa]	ν_{LT}
unidirectional CFRP	160	17	12.65	0.22
cross-ply GFRP	20	20	7.5	0.3

In fact, the aforesaid joints have in practice the same generalized Dundurs parameters (see *Eq. 20*), as shown in Table 3.

Table 3. Dundurs parameters for the GFRP-araldite joint and for the CFRP-GFRP joint.

Joint	α	β	λ_a	ρ_a	λ_b	ρ_b
GFRP-araldite	0.42	0.195	0.105	1.386	1.00	1.00
CFRP-GFRP	0.418	0.195	0.106	1.386	1.00	1.03

The photoelastic analysis has been performed on two different double lap joints between unidirectional GFRP (outer adherent) and araldite (inner adherent, see fig.5); in detail, in the outer composite adherent of the first joint the glass fibers are aligned with the longitudinal direction, whereas in the outer composite adherent of the second joint the glass fibers are oriented at 90°.

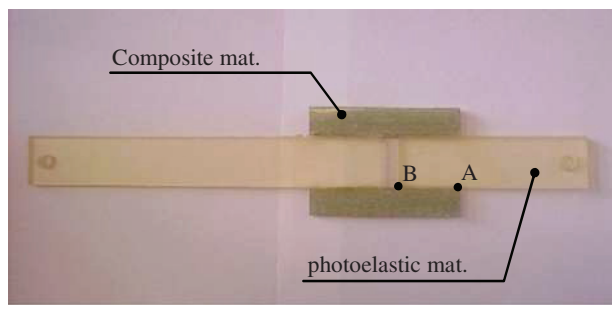

Fig. 5 – Picture of the araldite-GFRP co-cured joint used in the photoelastic analysis.

Fig. 6 shows the trend of the singularity orders ω_1 and ω_2 near the point A of fig. 5, varying the angle γ between the fiber orientation and the longitudinal direction of the joint.

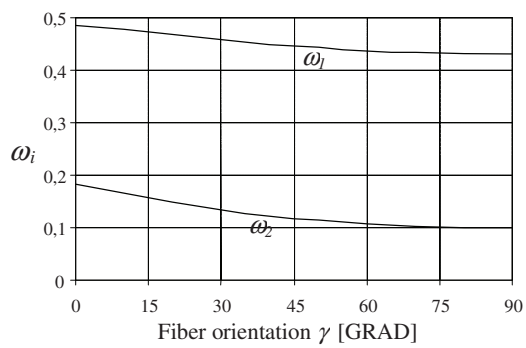

Fig. 6 – Singularity orders at the interface near the point A, varying the angle γ between the fibers and the longitudinal direction of the joint.

As shown in fig. 6, the singular stress field near the point A is characterized by two singularity orders in the plane for both the analyzed cases (γ=0° and γ=90°). Therefore, in this point the singular stress field is described by the binomial equation *(21)*.

Once the singularity orders are determined by using the procedure seen above and the angular function are evaluated by means of the procedure described in [33], it is possible to calculate the stress intensity factors K_1 and K_2. In detail, for the remote stress σ_o=1 MPa applied to the joint, the numerical analyses provide K_1=1.157 MPa mm$^{0.486}$ and K_2=-0.34 MPa mm$^{0.184}$ for the joint with composite adherent fibers aligned to the longitudinal direction whereas K_1=1.181 MPa mm$^{0.435}$ and K_2=-0.89 MPa mm$^{0.099}$ are provided for the joint with composite fibers at 90°.
Stress intensity factors can be obtained experimentally by using the digital photoelasticity [34]. Obviously, the comparison between the GSIFs obtained numerically and those obtained experimentally allows the user to estimate the approximations involved into both theoretical and numerical calculations performed by assuming the composite laminate as a homogeneous material characterized by the global elastic parameters, and neglecting the resin layer at the interface. The digital photoelasticity allows the user to obtain the GSIFs by means of the knowledge of the retardation δ, which depends on the stress field following the well-known equation:

$$\delta = \frac{C\,d}{\lambda}(\sigma_1 - \sigma_2) \tag{24}$$

where C is the birefringence constant of the photoelastic material, d is the thickness of the model, λ is the wavelength of the polariscope light source, σ_1 and σ_2 are the principal stresses.
In the binomial case, by substituting *Eq.(21)* into *Eq.(24)*, it is possible to write the retardation δ as a function of the stress intensity factors, the singularity orders and the angular functions, as [9]:

$$\delta^2(r,\vartheta) = K_1^2 L_1(\vartheta) r^{-2\omega_1} + K_2^2 L_2(\vartheta) r^{-2\omega_2} + K_1 K_2 L_3(\vartheta) r^{-(\omega_1+\omega_2)} \tag{25}$$

In the *Eq.(25)*, the angular functions L_1, L_2 and L_3 are given respectively by:

$$L_1(\vartheta) = \left(\frac{C\,d}{\lambda}\right)^2 \left\{ \left[f_{\vartheta\vartheta,1,1}(\vartheta) - f_{rr,1,1}(\vartheta) \right]^2 + 4\left[f_{r\vartheta,1,1}(\vartheta) \right]^2 \right\} \tag{26}$$

$$L_2(\vartheta) = \left(\frac{C\,d}{\lambda}\right)^2 \left\{ \left[f_{\vartheta\vartheta,1,2}(\vartheta) - f_{rr,1,2}(\vartheta) \right]^2 + 4\left[f_{r\vartheta,1,2}(\vartheta) \right]^2 \right\} \tag{27}$$

$$L_3(\vartheta) = \left(\frac{C\,d}{\lambda}\right)^2 \left\{ 2\left[f_{\vartheta\vartheta,1,1}(\vartheta) - f_{rr,1,1}(\vartheta) \right] \cdot \left[f_{\vartheta\vartheta,1,2}(\vartheta) - f_{rr,1,2}(\vartheta) \right] + 8 f_{r\vartheta,1,1}(\vartheta) f_{r\vartheta,1,2}(\vartheta) \right\} \tag{28}$$

Fixed the angle θ, the *Eq.(25)* is a polynomial function of r, which coefficients are obtained by the theoretical analysis. It implies that, considering a virtual radial line (θ=constant) inside the photoelastic material (starting from the singularity point - see fig. 7a), the curve δ^2 is described by a polynomial function of three terms having the following exponent: $-2\omega_1$, $-2\omega_2$ and $-(\omega_1+\omega_2)$.
This property allows the user to evaluate the stress dominated zone (SDZ) as the part of the curve δ^2 which is well interpolated by a polynomial function as:

$$y = l_1 r^{-2\omega_1} + l_2 r^{-2\omega_2} + l_3 r^{-(\omega_1+\omega_2)} \tag{29}$$

where, in accordance with the *Eq.(24)*, the factor l_3 is $l_3 = \pm L_3\,[l_1 l_2/(L_1 L_2)]^{1/2}$. After the determination of the SDZ, the value of the two SIFs can be computed by comparing *Eq.(29)* with *Eq.(25)*. It follows:

$$K_1 = \sqrt{\frac{l_1}{L_1}} \tag{30}$$

$$K_2 = \pm\sqrt{\frac{l_2}{L_2}} \tag{31}$$

where the correct sign of the *Eq.(31)* is equal to the sign of l_3 in the *Eq.(29)*. Fig. 7 shows the application of this procedure to the unidirectional GFRP/araldite joint with fibers aligned with the longitudinal direction of the joint, loaded with a total force of 1027 N.

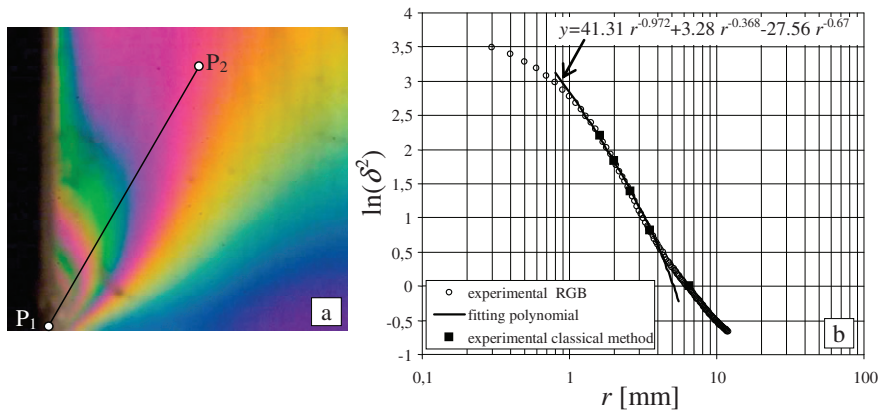

Fig. 7 – Photoelastic analysis: (a) isochromatic map in white light and (b) fringe order along the line P_1-P_2 near the point A for the joint with composite adherents fibers oriented at 0°.

In detail, fig. 7(a) shows the isochromatic map observed in the photoelastic material in white light near the point A, whereas the fig. 7(b) shows the square of the fringe order obtained by considering a radial line oriented at 30° with respect to the interface between the adherents (line P_1-P_2). By means of the procedure above described, the values of l_1, l_2 and l_3 are obtained (respectively 41.31, 3.28 and -27.56), whereas the theoretical analysis provides $L_1(30°)=0.868$ and $L_2(30°)=0.647$. As a consequence, by *Eq.(30)* and *Eq.(31)* the GSIFs for a longitudinal tension remote stress of 1 MPa, are computed as $K_1=1.148$ MPa mm$^{0.486}$ and $K_2=-0.37$ MPa mm$^{0.184}$. Fig. 8 shows the same procedure applied to the joint with fibers of the composite adherent oriented at 90°.

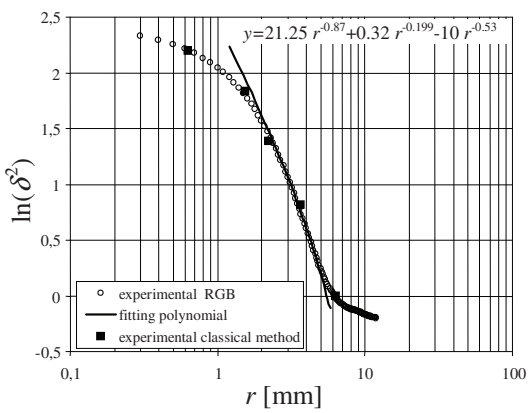

Fig. 8 – Fringe orders along the line P_1-P_2 near the point A for the joint with fibers of the composite adherent oriented at 90°.

In this case the following values have been obtained: l_1 =21.25, l_2 = 0.32 and l_3 =-10; the theoretical analysis provides instead $L_1(30°)=0.397$ and $L_2(30°)=0.685$. As a consequence, the GSIFs relate to a remote stress equal to 1 MPa take the following values: $K_1=1.215$ MPa mm$^{0.435}$ and $K_2=-0.11$ MPa mm$^{0.099}$.

The comparison between numerical and experimental values of the GSIFs is shown in Table 4. This comparison shows that the experimental results agree well with the numerical ones regarding K_1 (percentage error lower than 5%), whereas bigger differences are observed by comparing $K_{2,num}$ and $K_{2,exp}$. It is important to note that in this case such differences are not due to the influence of the resin layer but mainly to the ill-conditioned of *Eq.(25)* due to the very small contribution of the terms related to the second singularity order (small value of ω^2). In both the examined case, the good agreement between the first order GSIFs $K_{1,num}$ and $K_{1,exp}$ allows to affirm that for a common co-cured joint having t_a<0.1 mm, both theoretical and numerical analyses can be performed by neglecting the influence of the resin layer, i.e. by considering the ideal bi-material joint in which the interface lamina is correctly characterized by the global elastic constants determined experimentally or provided by micromechanics.

Table 4 – Comparison between numerical and experimental values of SIFs.

	Numerical		Experimental		Percentage error	
JOINT	$K_{1,num}$	$K_{2,num}$	$K_{1,exp}$	$K_{2,exp}$	$100(K_{1,exp}- K_{1,num})/ K_{1,num}$	$100(K_{2,exp}- K_{2,num})/ K_{2,num}$
GFRP 0°-araldite	1.157	-0.34	1.148	-0.37	-0.77 %	8.8 %
GFRP 90°-araldite	1.181	-0.89	1.215	-0.11	2.87 %	-87.6 %

Conclusions

The theoretical, numerical and experimental study of double lap hybrid metal-composite co-cured joints performed in this work, has shown that in general the influence of the interface resin layer on the generalized stress intensity factor values (GSIFs) that govern the interface singular stress field, is negligible. In particular, such a result is accurate for a common co-cured joint characterized by a resin layer thickness less than 0.1 mm. As a consequence, it is possible to state that the theoretical analyses and the numerical simulations of hybrid metal-composite co-cured joints can be in general performed correctly by considering an ideal bi-material joint without an adhesive layer at the interface. In other words, the interface lamina of the composite adherent can be accurately modeled (numerically or theoretically) as a homogeneous material characterized by the global elastic properties obtained experimentally or by micromechanics analysis. Also, by using the generalized Dundurs parameters, the digital photoelasticity can be used for the accurate experimental analysis of the GSIFs of a generic co-cured joint by investigating the equivalent photoelastic joint. The accuracy of the GSIFs obtained in this work for several co-cured joints by using the digital photoelasticity shows that such an experimental approach allows the user to determine the GSIFs of a generic co-cured joint between anisotropic materials by studying the equivalent joint having an adherent made by an isotropic birefringence material.

References

[1] Kim K.S., Yoo J.S., Yi Y.M., Kim C.G. Failure Mode and Strength of Unidirectional Composite Single Lap Bonded Joints with Different Bonding Methods. *Composite Structures.* 2006;**72**:477-485.

[2] Shin K.C., Lee J.J. Predictio,n of the Tensile Load-bearing Capacity of a Co-cured Single Lap Joint Considering Residual Thermal Stresses. *J. Adhesion of Science and Technology.* 2000;**14,13**:1691-1704.

[3] Shin K.C., Lee J.J. Tensile Load-bearing Capacity of Co-cured Double Lap Joints. *J. Adhesion of Science and Technology*. 2000; **14,12**:1539-1556.

[4] Shin K.C., Lee J. J. Fatigue Characteristics of a Co-cured Single Lap Joint Subjected to Cyclic Tensile Loads. *J. Adhesion Sci. Technol*. 2002;**16,4**:347-359.

[5] Shin K.C., Lim J. O., Lee J. J. The Manufacturing Process of Co-cured Single and Double Lap Joints and Evaluation of the Load Bearing Capacities of Co-cured Joints. *Journal of Materials Processing Technology*. 2003;**138**:89-96.

[6] Shin K. C., Lee J. J. Bond Parameters to Improve Tensile Load Bearing Capacities of Co-cured Single and Double Lap Joints with Steel and Carbon Fiber-epoxy Composite Adherends. *Journal of Composite Materials*. 2003;**5**:401-420.

[7] Suo Z. Singularities, Interfaces and Cracks in Dissimilar Anisotropic Media. *Proceeding of the Royal Society of London. Series A, Mathematical and Physical Sciences*. 1990;**427,1873**:331-358.

[8] Rice J.R., Sih G.C. Plane Problems of Cracks in dissimilar Media. *Journal of Applied Mechanics*. 1965;**32**:418-423.

[9] Zuccarello B., Ferrante S. Use of Automated Photoelasticity to Determine Stress Intensity Factors of Bimaterial Joints. *J. Strain Analysis*. 2005;**40,8**:785-800.

[10] Trantina G.G. Fracture Mechanics Approach to Adhesive Joints. *J. Composite Materials*. 1972;**6**:192-207.

[11] Suo Z., Hutchinson J.W. Sandwich Test Specimens for Measuring Interface Crack Toughness. *Materials Science and Engeneering*. 1989;**A107**:135-143.

[12] Suo Z. Failure of Brittle Adhesive Joints. *Applied Mechanics Rev. 1990 Supplement*. 1990;**43,5**:S276-S279.

[13] Santhanam S. A method to extract intensity factors for bimaterial problems using interlayer. *International Journal of Fracture*. 2005;**135**:137-159.

[14] Rice J.R. Elastic Fracture Mechanics Concepts for Interfacial Cracks. *Journal of Applied Mechanics*. 1988;**110**:98-103.

[15] Charalambides P.G., Lund J., Evans A.G., McMeeking, R.M. A test specimen for determining the fracture resistance of bimaterial interfaces. *Journal of Applied Mechanics*. 1989;**56,1**:77–82.

[16] Crews J.H., Shivakumar Jr.K.N., Raju I.S. Factors Influencing Elastic Stresses in Double Cantilever Beam Specimens; Adhesively Bonded Joints: Testing, Analysis and Design, *ASTM STP 981, W.S. Johnson ed.*, Philadelphia, PA: ASTM; 1988, p. 119-132.

[17] Penado F.E. A Closed Form Solution for the Energy Release Rate of the Double Cantilever Beam Specimen with an Adhesive Layer. *Journal of Composite Materials*. 1993;**27,4**:383-407.

[18] Kanninem M.F. An Augmented Double Cantilever Beam Model for Studying Crack Propagation and Arrest. *International Journal of Fracture*. 1973;**9**:83-92.
[19] Suo Z., Bao G., Fan B., Wang T.C. Orthotropy Rescaling and Implications for Fracture in Composites. *International Journal of Solids and Structure*. 1991;**28,2**:235-248.
[20] Wang X., Agrawal C.M. Interfacial Fracture Toughness of Tissue-Biomaterial Systems. *J Biomed Mater Res Appl Biomater*. 1997;**38**:1-10.
[21] Wang X., Agrawal C.M. A Mixed Mode Fracture Toughness Test of Bone-Biomaterial Interfaces. *J. Biomed Mater Res Appl Biomater*. 2000;**53**:664-772.
[22] Lekhnitskii, S.G. *Anisotropic Plates*, Translated from the Second Russian Edition by Tsai S.W. and Cheron T. Gordon and Beach Science Publisher Inc. New York, 1968.
[23] Eshelby J.D., Read W.T., Shockley W. *Acta Metall*. 1953;**1**:251-259.
[24] Stroh A.N. *Phil. Mag.* 1958;**7**:625-646.
[25] Muskhelishvili N.I. *Some basic problems of the mathematical theory of elasticity*. Groningem, Holland: P. Noordhoff Ltd; 1953.
[26] Dundurs J. Discussion of edge-bonded dissimilar orthogonal elastic wedges under normal and shear loading. *J. Appl. Mech*. 1969;**36**:650-652.
[27] Cherkaev A., Lurie K., Milton G.W. Invariant properties of the stress in plane elasticity and equivalence classes of composites. *Proc. R. Soc*. 1992;**A,438**:519-529.
[28] Moran B., Gosz M. Stress invariance in plane anisotropic elasticity. *Modelling Simul. Mater. Sci. Eng*. 1994;**2**:677-688.
[29] Williams M.L. Stress Singularities Resulting from Various Boundary Conditions in Angular Corners of Plates in Extension. *J. Appl. Mech.* 1952; **19**:526-528.
[30] Carpinteri A. Stress-singularity and Generalized Fracture Toughness at the Vertex of Re-entrant Corners. *Engineering Fracture Mechanics.* 1987; **26**:143-155.
[31] Broek D. *Elementary Engineering Fracture Mechanics*. Dordrecht, The Netherlands: Martinhus Nijhoff; 1987.
[32] Broek D. *Practical Use of Fracture Mechanics*. Dordrecht, NL: Kluver Academic Publisher; 1988.
[33] Pageau S.S., Kesavaram S.G., Sherril B.B., Paul F.J. Standardized Complex and Logarithmic Eigensolutions for n-material Wedges and Junctions. *Int. J. Fract.* 1996:**77**;51-76.
[34] Ramesh K., Mangal S. K. Data acquisition techniques in digital photoelasticity: a review. *Optics and Lasers in Engineering*. 1998:**30**;53-75.